COSMIC ORIGINS SPECTROGRAPH OBSERVATIONS OF THE CHEMICAL COMPOSITION OF LMC N132D.[1]

Kevin France[2], Matthew Beasley, Brian A. Keeney, Charles W. Danforth, Cynthia S. Froning, and James C. Green

Center for Astrophysics and Space Astronomy, 389 UCB, University of Colorado, Boulder, CO 80309
Draft version September 22, 2009

ABSTRACT

We present new far-ultraviolet spectra of an oxygen-rich knot in the Large Magellanic Cloud supernova remnant N132D, obtained with the *Hubble Space Telescope*-Cosmic Origins Spectrograph. Moderate resolution ($\Delta v \approx 200$ km s^{-1}) spectra in the *HST* far-ultraviolet bandpass ($1150 \lesssim \lambda \lesssim 1750$ Å) show emission from several ionization states of oxygen as well as trace amounts of other species. We use the improvements in sensitivity and resolving power offered by COS to separate contributions from different velocity components within the remnant, as well as emission from different species within the oxygen-rich knot itself. This is the first time that compositional and velocity structure in the ultraviolet emission lines from N132D has been resolved, and we use this to assess the chemical composition of the remnant. No nitrogen is detected in N132D and multiple carbon species are found at velocities inconsistent with the main oxygen component. We find helium and silicon to be associated with the oxygen-rich knot, and use the reddening-corrected line strengths of O III], O IV], O V, and Si IV to constrain the composition and physical characteristics of this oxygen-rich knot. We find that models with a silicon-to-oxygen abundance ratio of $N(\text{Si})/N(\text{O}) = 10^{-2}$ can reproduce the observed emission for a shock velocity of ≈ 130 km s^{-1}, implying a mass of ~ 50 $M_\odot$ for the N132D progenitor star.

Subject headings: supernovae: individual (LMC N132) — ISM: supernova remnants — ultraviolet: ISM

1. INTRODUCTION

Oxygen-rich supernova remnants (SNRs) are a category of young remnants characterized by enhanced abundances of oxygen, neon, and other heavy elements, and are observed to have large outflow velocities ($v \geq 1000$ km s^{-1}). O-rich remnants are thought to be the ejected stellar interiors from helium-burned layers of massive (≥ 10 M$_\odot$) progenitor stars. These objects are ideal for studies of the evolution of massive stars and stellar nucleosynthesis. O-rich SNRs are found locally (e.g., Cassiopaiea A; Chevalier & Kirshner, 1979) as well as in nearby galaxies (e.g., Blair et al. 2000).

Far-ultraviolet (far-UV) spectra of these objects provide a rich set of diagnostic lines for determining the composition and physical state of the stellar material. Far-UV observations probe excitation mechanisms and shock physics, providing a quantitative observational basis for studies of the interaction between supernovae and the interstellar medium. However, the accessibility of these objects varies widely depending on the foreground extinction to a given SNR. The majority of Galactic SNRs are strongly reddened, making studies of local O-rich ejecta challenging. O-rich SNRs beyond the Local Group of galaxies cannot be spatially resolved. The Magellanic Clouds offer the best compromise of low reddening and spatially resolvable targets suitable for far-UV investigations. Well studied O-rich remnants include N132D and SNR 0540 in the LMC, and E0102 in the SMC.

The young, oxygen-rich SNR N132D is located in the bar of the Large Magellanic Cloud (LMC) and was first identified as a supernova remnant by Westerlund & Mathewson (1966). Danziger & Dennefeld (1976) and Lasker (1978) confirmed its oxygen-rich nature. Spectroscopic studies (Danziger & Dennefeld 1976; Lasker 1980; Dopita & Tuohy 1984) revealed high-velocity filaments showing optical emission from oxygen and neon only spanning a total velocity range of $\sim$ 4400 km s^{-1}. The oxygen-rich filaments are concentrated near the middle of the remnant (Borkowski et al. 2007). Outside the fast-moving material is a bright x-ray shell (Long et al. 1981; Mathewson et al. 1983) that is associated with an optical emission line rim (Hughes 1994; Blair et al. 1994) of radius $\sim$ 1 arcminute ($\sim$ 13 parsecs). Dickel & Milne (1995) observed 6 centimeter radio emission that coincides with the x-ray shell.

Blair et al. (2000) found that the abundances derived for the ejecta in N132D roughly match models of a star with an initial mass of 35 M$_\odot$ with the following condition: the O-rich mantle of the progenitor star did not mix with deeper O-burning layers. If there had been mixing between these layers, sulfur and silicon would have been added to the ejecta. They conclude that the ejecta is comprised of oxygen, neon, carbon, and magnesium, which may indicate that the progenitor was a WO Wolf-Rayet star, perhaps with a mass as high as 85 M$_\odot$ (Woosley et al. 1995).

In this paper, we expand on previous observations of N132D. We present first results from the Cosmic Origins Spectrograph (COS), recently installed on the *Hubble Space Telescope* (*HST*). We use these data to resolve the composition of the O-rich knot in N132D, and evaluate the mass of the progenitor star based on the ele-
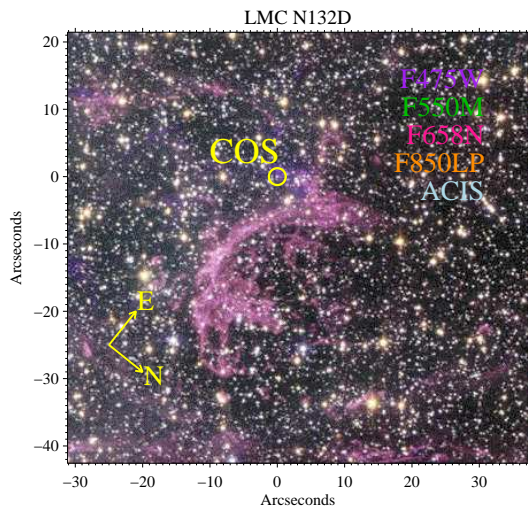
FIG. 1.— The inner shock region of the N132D SNR observed by the Cosmic Origins Spectrograph. The COS aperture is shown overlaid on the O-rich knot shown at the origin (R.A. = 05^h 25^m 25.51^s, Dec. = -69° 38′ 14.0″; J2000) of this composite optical/X-ray image from *HST*-ACS and *Chandra*-ACIS.
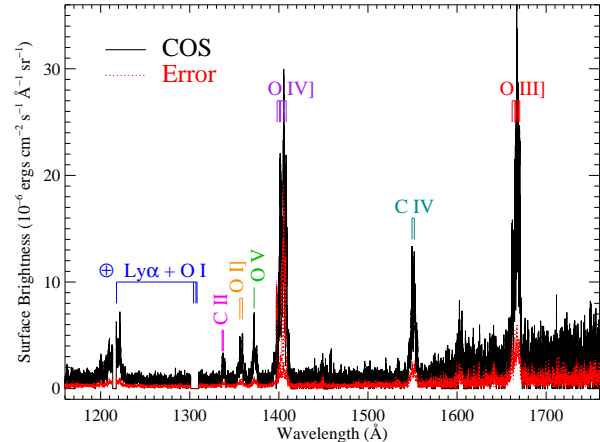

FIG. 2.— The full COS spectrum of N132D-P3, obtained with the G130M and G160M modes. Several ionization states of oxygen are observed and emission from Si IV (blended with O IV] λ1400; Figure 3) is detected for the first time. The oxygen and silicon are found at a common velocity; however, a velocity offset of the carbon species suggests that the carbon is spatially distinct from the O-rich knot. Lines from geocoronal H I and O I have been removed.

mental abundances of the stellar ejecta. We describe the COS observations and custom data reduction in §2. A quantitative analysis of the far-UV spectrum is presented in §3. In §4, we compare the measured line strengths to shock models to constrain the post-explosion abundances and the mass of the N132D progenitor star.

2. *HST*-COS OBSERVATIONS AND DATA REDUCTION

The Cosmic Origins Spectrograph is a slitless, modified Rowland Circle spectrograph designed for high-sensitivity observations of point sources in the vacuum-ultraviolet bandpass (1150 – 3200 Å). COS is optimized for deep, moderate-resolution spectroscopy (R $\cong$ 20,000; $\Delta v \approx$ 15 km s^{-1} for point source observations) in the far-UV (1150 $\lesssim \lambda \lesssim$ 1750 Å). The far-UV channel employs a single optical element for dispersion, focus, and correction of the spherical aberration of the *HST* primary mirror. A pre-flight review of COS can be found in Green et al. (2003) and a full instrument description and on-orbit performance characteristics are in preparation (Green et al.; Osterman et al. - in prep).

COS was installed on *HST* during STS-125/Servicing Mission 4 (SM4) in 2009 May. The O-rich knot in N132D was observed by COS on 2009 August 10 and 31 as part of the Early Release Observation program (*HST* proposal ID 11503; datasets `lacc01` and `lacc51`). Spectroscopic data was obtained on N132D over 5 orbits, using both far-UV medium-resolution gratings (G130M and G160M) to provide continuous spectral coverage from $\sim$ 1150 – 1750 Å. The pointng (R.A. = 05^h 25^m 25.51^s, Dec. = -69°38′14.0″; J2000) is coincident with previous far-UV spectroscopic observations made by *IUE* (position 'P1' of Blair et al. 1994) and *HST*-FOS (position 'P3' of Blair et al. 2000). The pointing is shown in Figure 1, with the COS aperture (2.5″ diameter) overlaid on a composite *HST/Chandra* image of the region. The to-

tal exposure times were 5190 and 4770 seconds for the G130M and G160M modes, respectively. In order to achieve continuous spectral coverage and minimize fixed pattern noise, observations in each grating were made at four separate central wavelength settings (λ1291, 1300, 1309, and 1318 in G130M and λ1589, 1600, 1611, and 1623 in G160M).

Observations made during the SM4 observatory verification period (SMOV) were not processed with the complete, flight-qualified version of the COS calibration pipeline, CALCOS[3]. Custom processing was performed to properly extract, calibrate and coadd the N132D data set. The detector coordinates used by CALCOS for extracting 1-dimensional (λ vs. F_λ) spectra from the 2-dimensional spectrogram are optimized for point sources, hence custom extraction windows were used to define proper target and background regions for this filled-aperture observation. A correction for spectral drift during the exposure was made by referencing an on-board calibration lamp. Finally, pulse height screening was performed in order to remove detector hot spots and other spurious events on the microchannel plates from the final spectrum. Spectra from individual exposures were then cross-correlated and coadded onto a common wavelength grid. The full far-UV spectrum of N132D is shown in Figure 2 with nebular emission lines labeled. The minimum spectral resolution is observed to be $\Delta v \sim$ 200 km s^{-1}, corresponding to the expected COS extended source resolving power for the medium-resolution grating modes (R $\approx$ 1500).

3. ANALYSIS AND RESULTS

3.1. *Nebular Species and Velocity Separations*

[3] We refer the reader to the COS Data Handbook for more details: www.stsci.edu/hst/cos/documents/handbooks/ datahandbook/COS_longdhbcover.html
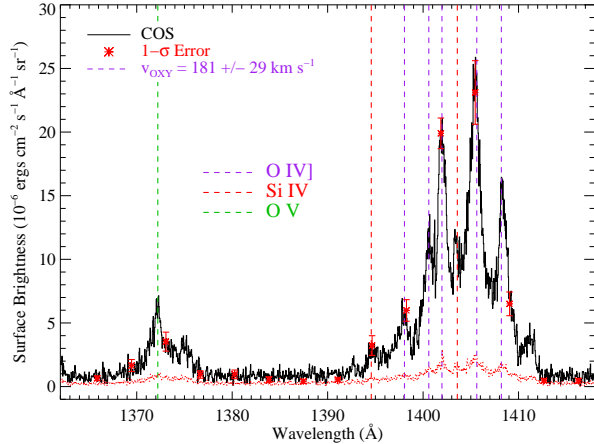
FIG. 3.— The spectrum of N132D in the 1362 – 1418Å window. The data allow us to separate the contributions from oxygen and silicon in this knot for the first time. The different ionization states of oxygen as well as the emission from Si IV are located at a common velocity, listed in Table 1.

TABLE 1
OBSERVED ATOMIC LINE STRENGTHS OF THE O-RICH KNOT IN N132D.

Species[a]	λ_{obs} (Å)	Line Flux[b]	FWHM[c] (km s^{-1})	Δv[d] (km s^{-1})
unID	1221.62	3.84±0.81	258	...
C II	1336.64	1.23±0.66	172	476
C II	1337.69	1.42±0.69	326	445
O IV][e]	1339.17	1.42±0.19	202	126
O I]	1356.30	3.12±0.66	230	155
UnID	1357.71	1.17±0.92	141	...
O I]	1359.08	3.08±0.54	183	126
O V	1372.20	9.18±0.66	477	197
O Vr	1374.83	3.73±0.87	390	772
Si IV	1394.86	3.01±0.87	360	237
O IV]	1397.92	10.29±1.23	541	149
O IV]	1400.62	15.61±1.44	320	245
O IV]	1402.03	18.68±1.68	210	186
Si IV	1403.44	12.89±2.61	287	143
O IV]	1405.45	39.86±1.32	394	137
O IV]	1408.29	24.25±0.78	417	194
O IV]r	1411.10	4.08±0.56	281	793
C IV	1549.48	16.98±2.37	377	248
C IV	1552.16	19.83±2.70	476	267
C IVr	1554.91	4.58±1.32	187	799
unID	1603.04	6.81±1.92	544	...
unID	1605.87	3.28±1.80	341	...
He II	1640.31	5.73±0.72	748	143
O III]	1661.83	6.72±0.63	216	187
O III]	1665.15	15.03±0.99	340	189
O III]	1667.19	32.60±0.87	276	188
O III]	1668.63	12.61±1.38	222	164
O III]	1670.20	23.02±0.57	353	160

[a] Emission lines labeled as r trace a high-velocity component (788 ± 14 km s^{-1}) separate from the O-rich knot (181 ± 29 km s^{-1}).
[b] 10^{-6} ergs cm^{-2} s^{-1} sr^{-1}
[c] The linewidths measured from a multiple Gaussian fitting procedure are estimated to have a 1-σ uncertainty of ± 100 km s^{-1}.
[d] Velocity shift from the rest wavelength,
$\Delta v = (\lambda_{obs} - \lambda_{rest}) \times (c/\lambda_{rest})$.
[e] Tentative identification.

The narrow-band WFPC2 (Morse et al. 1996) and multi-band ACS images (Figure 1) clearly indicate that the O-rich knot targeted by COS has a substantially different composition than other regions of the remnant. This is attributable to the degree of mixing between the stellar ejecta and the ambient pre-supernova medium, both interstellar and from earlier mass loss episodes of the progenitor star. The sensitivity and spectral resolving power of COS enable us to separate the emission from individual species unambiguously and quantify the velocity offsets between these components. We find oxygen to dominate the emission from this knot, consistent with previous findings (Blair et al. 1994; Morse et al. 1996; Blair et al. 2000; Borkowski et al. 2007). We observe oxygen in four ionization states (O I, O III, O IV, and O V), as well as emission from C II λλ1334/1335, C IV λλ1548/1550, smaller amounts of Si IV λλ1394/1403, He II λ1640, and several unidentified lines (Table 1).

Line centers, widths, and integrated strengths are determined from Gaussian fits to the data. We employ a modified version of the MPFIT IDL routine that accommodates interactive fitting of multiple lines simultaneously. On-orbit flux calibration files were not available during SMOV, and we added 25% to the error in the line-strengths quoted in Table 1. In order to establish the velocity of the O-rich knot, we assumed that the higher ionization states of oxygen were representative. The heliocentric velocity of the O III, O IV, and O V components is 181 ± 29 km s^{-1}. Within the uncertainties of the fitting procedure, this implies that the O I, Si IV, and He II are all at the velocity of knot, which we interpret as evidence for the cospatiality of these species. A 56 Å window of the spectrum including O V, Si IV, and O IV is shown in Figure 3, with dashed lines indicating the expected locations of the lines relative to their rest wavelengths.

The carbon components are found at significantly different velocities, 461 and 258 km s^{-1} for v_{CII} and v_{CIV}, respectively. In addition to the separation seen in the carbon species, we also find weaker high-velocity emission components on the red wing of three line complexes. There are high-velocity components associated with C IV, O IV, and O V, all consistent with a velocity of 788 km s^{-1}. Interestingly, we do not observe a high-velocity component in O III. Nitrogen is not detected in any ionization state in our dataset. We place an upper limit on the line flux from N V λλ1238/1242 of 2 × 10^{-6} ergs cm^{-2} s^{-1} sr^{-1}, a factor of ∼ 30 lower than the upper limit presented by Blair et al. (2000).

We take these distinct velocity components as representative of the composition of the O-rich knot. The knot is predominantly oxygen, with trace abundances of helium and silicon. The carbon species and the emission associated with the high-velocity components are assumed to be spatially distinct from the O-rich knot and located in a different region of the remnant.

3.2. Reddening Correction

In order to make a meaningful comparison to the ultraviolet emission lines predicted by supernova remnant shock models (described in the following section), a correction must be made for the effects of differential extinction by interstellar dust. We carried out an extinc-
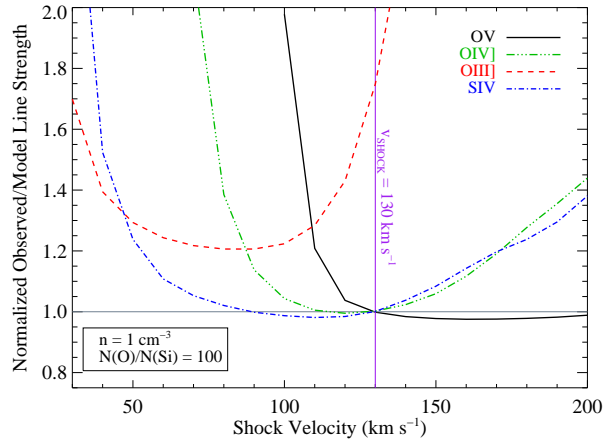
FIG. 4.— A comparison of the observed O V λ1372, O IV]+Si IV λ1400, and O III λ1664 line strengths with those predicted by the modified Raymond et al. (1979) model described in §4. The Observed/Model ratios were normalized to unity for O IV at $v_{SHOCK} = 130$ km s^{-1}. The model confirms the pre-shock density of $n = 1$ cm^{-3} and oxygen-to-silicon abundance ratio ($N(O)/N(Si) = 100$) used in Blair et al. (2000), and constrains the shock velocity in the highly ionized species. We use the $N(O)/N(Si)$ ratio in conjunction with an upper limit on $N(O)/N(C)$ to estimate the N132D progenitor mass to be ~ 50 $M_\odot$.

tion correction by assuming that all of the relevant dust was associated with the LMC and can be represented by the average 30 Doradus reddening curve (Fitzpatrick 1986). Taking $E(B - V) = 0.12$ with a selective extinction $R_V = 3.2$ (Blair et al. 2000), a continuous extinction curve is created for the COS bandpass. The line strengths are corrected by dividing by this curve in transmission space.

4. DISCUSSION

4.1. O-rich Shock Models and Physical Conditions in the Knot

We have compared the emission line strengths observed by COS with a grid of supernova shock models in order to constrain important physical quantities including the density of the preshock medium (n), the abundances of carbon and silicon relative to oxygen, and the shock velocity. We have used a modified version of the Raymond (1979) shock model code. This is the same code used to model the HST-FOS observations presented by Blair et al. (2000), and we refer the reader to that paper for details of the model. We ran this model in the weakly magnetized limit, with a pre-shock density of $n = 1$ cm^{-3} normalized at a shock velocity of $V_{SHOCK} = 100$ km s^{-1} for a constant ram pressure and a power-law index of $\alpha = 0.4$. We used the elemental abundances from Blair et al. (2000) for silicon ($N(O)/N(Si) = 10^2$) and from our COS-derived upper limit for carbon ($N(O)/N(C) \geq 10^2$). We ran a grid of models for values of $v_{SHOCK} = 30 - 200$ km s^{-1}, and tabulated the predicted far-UV emission line strengths in three ionization states of oxygen (O III, O IV, and O V) and Si IV.

The normalized ratios of observed/model line strengths

are shown in Figure 4. We find relatively good agreement between the model and observed line strengths with a shock velocity of $v_{SHOCK} = 130 \pm 20$ km s^{-1} for O V, O IV, and Si IV. The fit for the O III line strength is discrepant in both shock velocity and surface brightness. It is interesting to note that the $\sim 20\%$ offset for the O III line strength is exactly the same difference in the dust attenuation curve between 1400 and 1664 Å. We suggest that the extinction curve to N132D is significantly flatter than the typical 30 Doradus or LMC extinction curves, perhaps reflecting a depleted population of small dust grains ($R_V > 4.0$) on the sightline to this remnant. The O III appears to be more sensitive to slower shocks ($v_{SHOCK} \sim 80$ km s^{-1}, while the higher ionization traced by O V cannot be produced in shocks slower than ~ 100 km s^{-1}. Taken as a whole, these findings agree with a physical scenario where shocks of different velocities are seen superposed (Vancura et al. 1992) in this O-rich knot, which has a preshock density and silicon abundance consistent with those presented in Blair et al. (2000), while we rule out a substantial carbon abundance in this region.

4.2. Mass of the Progenitor Star

The relative abundances of the O-rich knot in N132D can be compared to models of massive stars and supernova explosions to constrain the mass of the progenitor star. It should be stressed that we are presenting an analysis of one small knot of ejecta in a much larger remnant. While we can use this information to place bounds on the progenitor star, it would be inappropriate to make definitive statements regarding the nature of the presupernova star based on such a small sample of the stellar core. With that caveat in mind, we find relatively good agreement between our abundances and those of the 40 $M_\odot$ main sequence model presented in Nomoto et al. (1997). Similar results are seen for the 70 $M_\odot$ star, but the lower $N(Si)/N(O)$ of the former model more closely reproduces our results. The 25 $M_\odot$ can be ruled out as it predicts too little silicon and $N(C)/N(Si)$ greater than unity. Blair et al. (2000) also comment on the 85 $M_\odot$ Wolf-Rayet B model (Woosley et al. 1993) with core masses from $2.7 \leq M_{CORE} \leq 7$ $M_\odot$ being a reasonable fit to the observations. This model has a relatively high $N(C)/N(O)$ (> 0.1). In light of the spatial separation of the carbon components, which could not be resolved in the FOS data, we consider this model to be ruled out. We note however, that for a narrow range of core mass (M_{CORE} 2.6 ± 0.1 $M_\odot$), the 60 $M_\odot$ Wolf-Rayet A model (the distinction between "A" and "B" in Woosley et al. 1993 is the reaction rate for the conversion of carbon to oxygen in the stellar core) provides a reasonable fit to the abundances. In this model, the relative silicon and carbon abundances are of order 10^{-2}, in agreement with the COS data. Additionally, more recent models by Umeda & Nomoto (2008) calculate abundances of oxygen and silicon in the post-explosion material for 50 and 100 $M_\odot$ main sequence stars. Their 50 $M_\odot$ model, with an explosion energy of 3×10^{52} ergs matches the $N(Si)/N(O)$ ratio for the O-rich N132D knot, while the post-explosion yields for a 100 $M_\odot$ star overpredict the silicon abundance by an order of magnitude. Given the findings described above, we adopt a mass of 50 ± 25 $M_\odot$ for the progenitor to the N132D supernova.

REFERENCES

Blair, W. P., Morse, J. A., Raymond, J. C., Kirshner, R. P., Hughes, J. P., Dopita, M. A., Sutherland, R. S., Long, K. S., & Winkler, P. F. 2000, ApJ, 537, 667

Blair, W. P., Raymond, J. C., & Long, K. S. 1994, ApJ, 423, 334

Borkowski, K. J., Hendrick, S. P., & Reynolds, S. P. 2007, ApJ, 671, L45

Chevalier, R. A. & Kirshner, R. P. 1979, ApJ, 233, 154

Danziger, I. J. & Dennefeld, M. 1976, ApJ, 207, 394

Dickel, J. R. & Milne, D. K. 1995, AJ, 109, 200

Dopita, M. A. & Tuohy, I. R. 1984, ApJ, 282, 135

Fitzpatrick, E. L. 1986, AJ, 92, 1068

Green, J. C., Wilkinson, E., & Morse, J. A. 2003, in Society of Photo-Optical Instrumentation Engineers (SPIE) Conference Series, Vol. 5164, Society of Photo-Optical Instrumentation Engineers (SPIE) Conference Series, ed. O. H. W. Siegmund, 17–23

Green, J. C. e. a. 2010, ApJ, 000, L1+

Hughes, J. P. 1994, in American Institute of Physics Conference Series, Vol. 313, The Soft X-ray Cosmos, ed. E. M. Schlegel & R. Petre, 144–+

Lasker, B. M. 1978, ApJ, 223, 109

—. 1980, ApJ, 237, 765

Long, K. S., Helfand, D. J., & Grabelsky, D. A. 1981, ApJ, 248, 925

Mathewson, D. S., Ford, V. L., Dopita, M. A., Tuohy, I. R., Long, K. S., & Helfand, D. J. 1983, ApJS, 51, 345

Morse, J. A., Blair, W. P., Dopita, M. A., Hughes, J. P., Kirshner, R. P., Long, K. S., Raymond, J. C., Sutherland, R. S., & Winkler, P. F. 1996, AJ, 112, 509

Nomoto, K., Hashimoto, M., Tsujimoto, T., Thielemann, F.-K., Kishimoto, N., Kubo, Y., & Nakasato, N. 1997, Nuclear Physics A, 616, 79

Osterman, S., J. C. e. a. 2010, ApJ, 000, L5+

Raymond, J. C. 1979, ApJS, 39, 1

Umeda, H. & Nomoto, K. 2008, ApJ, 673, 1014

Vancura, O., Blair, W. P., Long, K. S., & Raymond, J. C. 1992, ApJ, 394, 158

Westerlund, B. E. & Mathewson, D. S. 1966, MNRAS, 131, 371

Woosley, S. E., Langer, N., & Weaver, T. A. 1993, ApJ, 411, 823

—. 1995, ApJ, 448, 315